

$^3S_1 - ^3D_1$ coupled channel $\Lambda_c N$ interactions: chiral effective field theory vs. lattice QCDJing Song,^{1,2} Yang Xiao,^{1,2,3} Zhi-Wei Liu,² Kai-Wen Li,^{4,5,2,*} and Li-Sheng Geng^{2,6,7,†}¹*School of space and environment, Beihang University, Beijing, 102206, China*²*School of Physics, Beihang University, Beijing, 102206, China*³*Université Paris-Saclay, CNRS/IN2P3, IJCLab, Orsay, 91405, France*⁴*Medical Management Department, CAS Ion Medical Technology Co., Ltd., Beijing 100190, China*⁵*Beijing Advanced Innovation Center for Big Data-Based Precision Medicine,**School of Medicine and Engineering, Beihang University,**Key Laboratory of Big Data-Based Precision Medicine (Beihang University),**Ministry of Industry and Information Technology, Beijing, 100191, China*⁶*Beijing Key Laboratory of Advanced Nuclear Materials and Physics, Beihang University, Beijing, 102206, China*⁷*School of Physics and Microelectronics, Zhengzhou University, Zhengzhou, Henan, 450001, China*

(■Dated: October 25, 2022)

We study the lattice QCD $\Lambda_c N$ phase shifts for the $^3S_1 - ^3D_1$ coupled channel using both the leading order covariant chiral effective theory and the next-to-leading order non-relativistic chiral effective field theory. We show that although it is possible to describe simultaneously the 3S_1 and 3D_1 phase shifts and the inelasticity η_1 , the fitted energy range is pretty small, only up to $E_{c.m.} = 5$ MeV. This raises concerns regarding the consistency between leading/next-to-leading order chiral effective field theory and the lattice QCD simulations.

PACS numbers: 13.75.Ev, 12.39.Fe, 21.30.Fe

I. INTRODUCTION

The Λ_c baryon as the lightest charm baryon has attracted a lot of attention, which may exist in finite nuclei to form Λ_c hypernuclei. The HAL QCD Collaboration performed the first lattice QCD simulations of the $\Lambda_c N$ and $\Sigma_c N$ interactions for unphysical light quark masses ($m_\pi = 410, 570, 700$ MeV) [1], which provided vital information on the interaction between a nucleon and a charmed baryon Λ_c or Σ_c . Employing these lattice QCD results, extrapolations to the physical point have been performed using either the non-relativistic chiral effective field theory (ChEFT) at next-to-leading order (NLO) [2] or the covariant ChEFT at leading order (LO) [3]. In the covariant ChEFT, Lorentz covariance is maintained by employing the covariant chiral Lagrangians, the full form of Dirac spinors, and the relativistic scattering equation (the Kadyshevsky equation). It has been shown that the covariant ChEFT approach can provide reasonable descriptions of octet baryon-octet baryon interactions already at LO, including all the systems from strangeness $S = 0$ to $S = -4$, at least in the low energy region [4–14].¹ A recent study [11] showed that one could reproduce both the physical 1S_0 and $^3S_1 - ^3D_1$ and the lattice QCD nucleon-nucleon partial wave phase shifts fairly well. In particular, for the physical nucleon-nucleon phase shifts and lattice QCD data at $m_\pi = 469$ MeV, if one only fits to the 3S_1 phase shifts, the 3D_1 phase shifts and inelasticity η_1 can be predicted and vice versa, as shown in Ref. [16]. It implies that indeed the correlations induced by the imposed constraint of covariance in the covariant chiral potentials is reasonable.

In our previous study of the $\Lambda_c N$ interaction in the covariant ChEFT [3], the low energy constants (LECs) were determined by fitting to the lattice QCD data from the HAL QCD Collaboration, where the S -wave phase shifts up to $E_{c.m.} = 30$ MeV for $m_\pi = 410$ MeV and 570 MeV were considered. The results showed that the covariant ChEFT can describe the lattice QCD data fairly well at low energies. In addition, the phase shifts of the $\Lambda_c N$ 3D_1 partial wave and the inelasticity η_1 , as well as their physical counterparts were predicted.

In a recent study [17], it was shown that the predicted 3D_1 phase shifts by the NLO non-relativistic ChEFT are in agreement with the lattice QCD data of Ref. [18] at higher energies, but not those of Ref. [3]. A closer examination of the lattice QCD data revealed, however, that although at higher energies, the predictions of Ref. [3] do not agree with the lattice QCD data, but at low energies close to threshold, they do agree, both for the 3D_1 phase shifts and the inelasticity, at least qualitatively. On the other hand, the predictions of the NLO non-relativistic ChEFT [2] do not agree with the lattice QCD data at low energies.

In this work, we revisit the fits to the lattice QCD data and the corresponding extrapolations to the physical point. We study in detail the differences between the non-relativistic ChEFT and covariant ChEFT in the description of the $\Lambda_c N$ 3D_1 phase shifts

*E-mail me at: kaiwen.li@buaa.edu.cn

†E-mail me at: lisheng.geng@buaa.edu.cn

¹ The next-to-next-to-leading order relativistic chiral nucleon-nucleon interaction is shown to be able to describe the neutron-proton scattering phaseshifts up to $T_{lab.} = 200$ MeV as well as the next-to-next-to-next-to-leading order non-relativistic chiral nucleon-nucleon interactions. [15].

and inelasticity η_1 , including the effects of baryon masses and SD coupling in the contact terms, and the retardation effects in the one meson exchange term.² In addition, we study extrapolations to the physical point employing different fitting strategies to the lattice QCD data. These results are important to better understand the $\Lambda_c N$ interaction and might be helpful to guide future hypernuclei experiments.

The paper is organized as follows. In Sec. II, we briefly introduce the non-relativistic and the covariant chiral EFT. In Sec. III we perform fits to the lattice QCD data of Ref. [18], focusing on the low energy region, where ChEFT is expected to work. We summarize in Sec. IV.

II. THEORETICAL FRAMEWORK

In this section, we briefly introduce the non-relativistic ChEFT and covariant ChEFT for the $Y_c N$ interactions, where $Y_c = \Lambda_c, \Sigma_c$, and highlight the differences relevant for the present study.

In the non-relativistic ChEFT, the next-to-leading order potentials consist of non-derivative four-baryon contact terms (CT) and one-meson-exchanges (OME). The CT potentials for the 1S_0 and $^3S_1 - ^3D_1$ partial waves are [19]

$$\begin{aligned} V_{\text{CT},1S_0}^{Y_c N} &= \tilde{C}_1 s_0 + \tilde{D}_1 s_0 m_\pi^2 + (C_1 s_0 + D_1 s_0 m_\pi^2)(p^2 + p'^2), \\ V_{\text{CT},3S_1}^{Y_c N} &= \tilde{C}_3 s_1 + \tilde{D}_3 s_1 m_\pi^2 + (C_3 s_1 + D_3 s_1 m_\pi^2)(p^2 + p'^2), \\ V_{\text{CT},3D_1-3S_1}^{Y_c N} &= C_{\varepsilon_1} p'^2, \\ V_{\text{CT},3S_1-3D_1}^{Y_c N} &= C_{\varepsilon_1} p^2, \end{aligned} \quad (1)$$

where $p = |\mathbf{p}|$ and $p' = |\mathbf{p}'|$ are the initial and final center-of-mass (c.m.) momenta of the $Y_c N$ system, respectively. $\tilde{C}_i, \tilde{D}_i, C_i, D_i (i = ^1S_0, ^3S_1, \text{ and } \varepsilon_1)$ are LECs that need to be fixed by fitting to either experimental or lattice QCD data. The OME potential reads,

$$V_{\text{OME}}^{Y_c N \rightarrow Y'_c N} = -\frac{g_A^{Y_c Y'_c} g_A^{NN}}{4f_\pi^2} \frac{(\boldsymbol{\sigma}_1 \cdot \mathbf{q})(\boldsymbol{\sigma}_2 \cdot \mathbf{q})}{\mathbf{q}^2 + m_\pi^2} \times \mathcal{I}_{Y_c N \rightarrow Y'_c N}, \quad (2)$$

where $\mathbf{q} = \mathbf{p}' - \mathbf{p}$ is the transferred momentum. The coupling constants $g_A^{Y_c Y'_c}$ and g_A^{NN} and the isospin factor \mathcal{I} can be found in, e.g., Refs. [2, 20]. The scattering amplitudes are then obtained by solving the coupled-channel Lippmann-Schwinger equation,

$$T_{\rho'\rho}^{\nu'\nu,J}(p', p; \sqrt{s}) = V_{\rho'\rho}^{\nu'\nu,J}(p', p) + \sum_{\rho'', \nu''} \int_0^\infty \frac{dp'' p''^2}{(2\pi)^3} V_{\rho'\rho''}^{\nu'\nu'',J}(p', p'') \times \frac{2\mu_{\rho''}}{p_\rho^2 - p''^2 + i\eta} T_{\rho''\rho}^{\nu''\nu,J}(p'', p; \sqrt{s}), \quad (3)$$

where the labels ν, ν', ν'' denote the particle channels, ρ, ρ', ρ'' denote the partial waves, and μ_ρ is the pertinent reduced mass. The on-shell momentum in the intermediate state, p_ρ , is defined by $\sqrt{s} = \sqrt{M_{B_1,\rho}^2 + p_\rho^2} + \sqrt{M_{B_2,\rho}^2 + p_\rho^2}$. The potentials are regularized with an exponential form factor,

$$f_{\Lambda_F}(p, p') = \exp \left[-\left(\frac{p}{\Lambda_F} \right)^4 - \left(\frac{p'}{\Lambda_F} \right)^4 \right], \quad (4)$$

where Λ_F is the cutoff whose value is in the range of 500 – 600 MeV. The partial wave S matrix is related to the on-shell T matrix by

$$S_{\rho'\rho}^{\nu'\nu} = \delta_{\rho'\rho} \delta^{\nu'\nu} - 2ia T_{\rho'\rho}^{\nu'\nu}, \quad a = \frac{\sqrt{\mathbf{p}_{\text{cm}}^{\nu'} \mathbf{p}_{\text{cm}}^{\nu}} \mu^{\nu'\nu}}{16\pi^2}, \quad (5)$$

where \mathbf{p}_{cm} is the C.M. three-momentum of the $\Lambda_c N$ system. The phase space factor a is determined by the elastic unitarity of the scattering equation. For single channels, the phase shifts δ can be obtained from the on-shell S matrix,

$$S = \exp(2i\delta). \quad (6)$$

² We found that the retardation effects are quite small and therefore refrain from explicit discussions about these effects from now on, but they are always included in our study.

In order to calculate the phase shifts in coupled channels ($J > 0$), we use the “Stapp”- or “bar”- phase shifts parametrisation [21] of the S matrix, which can be written as

$$S = \begin{pmatrix} S_{--} & S_{-+} \\ S_{+-} & S_{++} \end{pmatrix} = \begin{pmatrix} \exp(i\delta_-) & 0 \\ 0 & \exp(i\delta_+) \end{pmatrix} \begin{pmatrix} \cos(2\epsilon) & i\sin(2\epsilon) \\ i\sin(2\epsilon) & \cos(2\epsilon) \end{pmatrix} \begin{pmatrix} \exp(i\delta_-) & 0 \\ 0 & \exp(i\delta_+) \end{pmatrix}, \quad (7)$$

where the subscript “+” is $J + 1$, “-” for $J - 1$. The resulting phase shifts and mixing angles are

$$\tan(2\delta_{\pm}) = \frac{\text{Im}(S_{\pm\pm}/\cos(2\epsilon_J))}{\text{Re}(S_{\pm\pm}/\cos(2\epsilon_J))}, \quad \tan(2\epsilon_J) = \frac{-iS_{+-}}{\sqrt{S_{++}S_{--}}}. \quad (8)$$

For more details about the non-relativistic ChEFT, please refer to Refs. [2, 17, 19, 20, 22–31].

In the covariant ChEFT, as discussed in Ref. [3], the 1S_0 and $^3S_1 - ^3D_1$ CT potentials for the $Y_c N$ system read,

$$\begin{aligned} V_{\text{CT},1S_0}^{Y_c N} &= \xi_{Y_c N} \left[C_{1S_0} \left(R_{p'}^N R_p^{Y_c} + R_p^N R_{p'}^{Y_c} \right) + C'_{1S_0} \left(R_{p'}^N R_p^N R_{p'}^{Y_c} R_p^{Y_c} + 1 \right) \right], \\ V_{\text{CT},3S_1}^{Y_c N} &= \frac{1}{9} \xi_{Y_c N} \left\{ 2(C_{1S_0} - C'_{1S_0}) \left(R_{p'}^{Y_c} R_p^{Y_c} - R_{p'}^N R_p^N \right) \right. \\ &\quad + C_{3S_1} \left(-6R_{p'}^N R_p^N + 9R_{p'}^N R_{p'}^{Y_c} + 9R_p^N R_p^{Y_c} + 6R_{p'}^{Y_c} R_p^{Y_c} \right) \\ &\quad \left. + 9C'_{3S_1} \left[R_{p'}^{Y_c} R_p^{Y_c} (R_{p'}^N R_p^N - 2) + 2R_{p'}^N R_p^N + 9 \right] \right\}, \\ V_{\text{CT},3D_1-3S_1}^{Y_c N} &= \frac{\xi_{Y_c N}}{9\sqrt{2}} \left\{ (C_{1S_0} - C'_{1S_0}) \left[R_p^N (R_{p'}^N + 3R_{p'}^{Y_c}) - R_{p'}^{Y_c} (3R_p^N + R_p^{Y_c}) \right] \right. \\ &\quad + C_{3S_1} \left[9R_p^{Y_c} (R_{p'}^N + 4R_p^N) + 3R_{p'}^N R_p^N - 3R_{p'}^{Y_c} (3R_p^N + R_p^{Y_c}) \right] \\ &\quad \left. + 9C'_{3S_1} \left\{ R_{p'}^{Y_c} [R_p^N (4R_{p'}^N R_p^{Y_c} + 3) + R_{p'}^{Y_c}] - R_p^N (R_p^N + 3R_p^{Y_c}) \right\} \right\}, \\ V_{\text{CT},3S_1-3D_1}^{Y_c N} &= \frac{\xi_{Y_c N}}{9\sqrt{2}} \left\{ (C_{1S_0} - C'_{1S_0}) \left[R_{p'}^N (R_p^N + 3R_p^{Y_c}) - R_{p'}^{Y_c} (3R_p^N + R_p^{Y_c}) \right] \right. \\ &\quad + C_{3S_1} \left[9R_{p'}^{Y_c} (R_p^N + 4R_{p'}^N) + 3R_p^N R_{p'}^N - 3R_p^{Y_c} (3R_{p'}^N + R_{p'}^{Y_c}) \right] \\ &\quad \left. + 9C'_{3S_1} \left\{ R_p^{Y_c} [R_{p'}^N (4R_p^N R_{p'}^{Y_c} + 3) + R_p^{Y_c}] - R_{p'}^N (R_{p'}^N + 3R_{p'}^{Y_c}) \right\} \right\}, \\ V_{\text{CT},3D_1}^{Y_c N} &= \frac{2}{9} \xi_{Y_c N} \left\{ (C_{1S_0} - C'_{1S_0} + 3C_{3S_1}) \left(R_{p'}^N R_p^N - R_{p'}^{Y_c} R_p^{Y_c} \right) \right. \\ &\quad \left. + 9C'_{3S_1} \left[R_{p'}^N R_p^N (4R_{p'}^{Y_c} R_p^{Y_c} - 1) + R_{p'}^{Y_c} R_p^{Y_c} \right] \right\}, \end{aligned} \quad (9)$$

where

$$\xi_{Y_c N} = 4\pi \frac{\sqrt{(E_{p'}^{Y_c} + M_{Y_c})(E_p^{Y_c} + M_{Y_c})(E_{p'}^N + M_N)(E_p^N + M_N)}}{4M_N M_{Y_c}} \quad \text{and} \quad R_{p(p')}^{Y_c, N} = \frac{p(p')}{E_{p(p')}^{Y_c, N} + M_{Y_c, N}}.$$

It should be noted that there exist three differences between the covariant and the non-relativistic ChEFT potentials as presented above: (1) the covariant chiral potentials explicitly contain the baryon masses M_{Y_c} and M_N , where $M_{Y_c} = (M_{\Lambda_c} + M_{\Sigma_c})/2$, whose values are the same as those given in Table I of Ref. [3]; (2) because of the fact $M_{Y_c} \neq M_N$, the LECs from the 1S_0 partial wave also contribute to those of the $^3S_1 - ^3D_1$ partial waves; (3) the LECs responsible for the SD coupling are correlated with those of the 1S_0 and 3S_1 potentials. It should be noted that the contributions from the $\Sigma_c N$ intermediate state in the CT potentials were set zero in both the non relativistic ChEFT [2] and covariant ChEFT [3], since the limited lattice QCD data could not fix these contributions.

The leading-order OME potential reads,

$$V_{\text{OME}}^{Y_c N \rightarrow Y_c' N} = -ig_A^{Y_c Y_c'} g_A^{NN} \bar{u}_{Y_c'}(p') \left(\frac{\gamma^\mu \gamma_5 q_\mu}{2f_\pi} \right) u_{Y_c}(p) \frac{i}{\Delta E^2 - q^2 - m^2 + i\epsilon}$$

$$\times \bar{u}_N(-p') \left(\frac{\gamma^\nu \gamma_5 q_\nu}{2f_\pi} \right) u_N(-p) \times \mathcal{I}_{Y_c N \rightarrow Y_c' N}, \quad (10)$$

where $\Delta E = E_{p'} - E_p$ is the transferred kinetic energy, i.e., the retardation effect, and we adopt the complete form of the Dirac spinor for the baryons involved

$$u_B(\mathbf{p}, s) = \left(\frac{1}{\frac{\boldsymbol{\sigma} \cdot \mathbf{p}}{E_p + M_B}} \right) \chi_s.$$

The coupled-channel Kadyshevsky equation [32] is solved to obtain the scattering amplitudes,

$$T_{\rho\rho'}^{\nu\nu',J}(p', p; \sqrt{s}) = V_{\rho\rho'}^{\nu\nu',J}(p', p) + \sum_{\rho'', \nu''} \int_0^\infty \frac{dp'' p''^2}{(2\pi)^3} \frac{M_{B_{1,\nu''}} M_{B_{2,\nu''}} V_{\rho\rho''}^{\nu\nu'',J}(p', p'') T_{\rho''\rho'}^{\nu''\nu',J}(p'', p; \sqrt{s})}{E_{1,\nu''} E_{2,\nu''} (\sqrt{s} - E_{1,\nu''} - E_{2,\nu''} + i\epsilon)}, \quad (11)$$

where \sqrt{s} is the total energy of the two-baryon system in the center-of-mass frame and $E_{n,\nu''} = \sqrt{p''^2 + M_{B_{n,\nu''}}^2}$, ($n = 1, 2$). In the numerical study, the potentials are regularized with the same exponential form factor as that of Eq. (4). The relation between the phase shifts and T -matrix is the same as explained above except for the phase space factor a , which appearing in the Kadyshevsky equation is $a = \frac{1}{8\pi^2} \frac{\sqrt{\mathbf{p}_{\text{cm}}^\nu \mathbf{p}_{\text{cm}}^{\nu'} M_{B_{1,\nu'}} M_{B_{2,\nu'}} M_{B_{1,\nu}} M_{B_{2,\nu}}}}{(E_{1,\nu'} + E_{2,\nu'})(E_{1,\nu} + E_{2,\nu})}$. More details about the covariant ChEFT approach can be found in Refs. [4–15].

III. FITTING PROCEDURE

In Ref. [33], the HAL QCD Collaboration presented the 1S_0 and 3S_1 phase shifts of the $\Lambda_c N$ interaction obtained from lattice QCD simulations with $m_\pi = 410, 570$, and 700 MeV. In addition, the corresponding 3D_1 partial wave phase shifts and inelasticity η_1 can be found in the Ph.D. thesis of Takaya Miyamoto [18]. The results show that the $\Lambda_c N$ 3D_1 phase shifts for $M_\pi = 410, 570$, and 700 MeV are slightly repulsive for the center of mass energy no larger than 15, 30, and 40 MeV, respectively and become attractive as $E_{\text{c.m.}}$ increases, and the inelasticity η_1 is close to unity in the whole energy region. Fittings to the S partial waves of $m_\pi = 410$ and 570 MeV (with $E_{\text{c.m.}} \leq 30$ MeV), and extrapolations to the physical point were performed in both the non-relativistic ChEFT [2] and covariant ChEFT [3]. The predictions for the 3D_1 phase shifts and inelasticity η_1 turn out to be dramatically different. The 3D_1 interaction in the former approach is attractive, while that in the latter is repulsive. In addition, both approaches predict a SD coupling stronger than that shown by the lattice QCD data.

In this study, we first investigate where such differences in the predicted $\Lambda_c N$ 3D_1 phase shifts between the two approaches originate. In particular, we focus on the masses of Y_c and N and the SD coupling in the CT potential. We note that there are no baryon mass terms in the CT potential of the non-relativistic ChEFT, while M_B (M_{Y_c} , M_N) appears in the baryon spinors of the covariant ChEFT. As $M_{Y_c} \geq M_N$, we used the “physical” masses for Y_c and N in our previous study, which has the consequence that C_{1S_0} (C'_{1S_0}) also contributes to the $^3S_1 - ^3D_1$ partial waves [3]. In addition, the SD coupling in the covariant ChEFT is correlated to the 3S_1 potential, while a free LEC appears in the non-relativistic ChEFT. These two differences lead to in total $2^2 = 4$ combinations that will be examined. In addition to our previous study [3], we perform three more fits to the same lattice QCD data, and make a systematic comparison of the results, to better understand how the results depend on the baryon masses and SD coupling in the CT potential.

Moreover, since both approaches fail to precisely reproduce the lattice QCD 3D_1 phase shifts of $\Lambda_c N$ at low energies, we adopt a new fitting strategy where the phase shifts of $\Lambda_c N$ 3S_1 , 3D_1 partial waves and inelasticity η_1 with $E_{\text{c.m.}} \leq 5$ MeV are simultaneously fitted. The new strategy can provide a closer look at the two approaches in the descriptions of low energy lattice QCD data. Note that we only consider the lattice QCD data with $m_\pi = 410$ and 570 MeV in all the aforementioned fittings. Details of the fitting strategies in this work are shown in Table I.

TABLE I: Seven fitting strategies studied in this work, where \checkmark indicates that the SD coupling in the CT potential is turned on, while \times denotes that the SD coupling is turned off in the covariant ChEFT approach.

Strategy	Lattice QCD data fitted	Approach	$M_{Y_c} [\] M_N$	SD coupling
1			\neq	\checkmark
2	3S_1	cov. ChEFT	\neq	\times
3	$E_{c.m.} \leq 30$ MeV		$=$	\checkmark
4			$=$	\times
5	${}^3S_1, {}^3D_1, \eta_1$	cov. ChEFT	\neq	\checkmark
6	$E_{c.m.} \leq 5$ MeV		$=$	\checkmark
7		non-rel. ChEFT		

IV. RESULTS AND DISCUSSIONS

A. Origin of the difference in predicting the $\Lambda_c N$ 3D_1 phase shifts

The fitted results of strategies 1 – 4 as described in the previous section are summarized qualitatively in Table II and quantitatively in Fig. 1. It is noted that the treatment of the potentials in strategy 1 is that adopted in Ref. [3]³, and strategy 4 is approximately the same as that of the non-relativistic ChEFT. The following conclusions can be obtained from the table: first, the baryon masses affect the 3D_1 phase shifts for the large pion mass ($m_\pi = 570$ MeV), where negative phase shifts are obtained in strategies 1, 2 and they become positive if M_{Y_c} is taken to be the same as M_N (strategies 3, 4). Second, only when $M_{Y_c} = M_N$ and the SD coupling in the CT potential is turned off, the 3D_1 interaction becomes attractive in the unphysical region (strategy 4). Third, the SD coupling in the covariant ChEFT reduces the attraction in the 3S_1 partial wave in the physical region, compared with the non-relativistic case, as shown in strategies 1 and 3.

TABLE II: Dependence of the $\Lambda_c N$ 3S_1 and 3D_1 phase shifts on the baryon masses and SD coupling for different pion masses (in units of MeV). The “+” and “−” indicate the sign of the $\Lambda_c N$ 3S_1 and 3D_1 phase shifts within the fitting region $E_{c.m.} \leq 30$ MeV, where “+” and “−” denote attractive and repulsive potentials, respectively. The values of the $\chi^2/\text{d.o.f.}$ (in units of 10^{-2}) are obtained with $\Lambda_F = 600/700$ MeV.

Strategy	$M_{Y_c} [\] M_N$	SD coupling	m_π	δ_{3S_1}	δ_{3D_1}	$\chi^2/\text{d.o.f.}^\dagger$
1	\neq	\checkmark	138	$+-^\dagger$	−	
			410	+	−	1.30/1.32
			570	+	−	25.9/30.9
2	\neq	\times	138	+	−	
			410	+	−	1.30/1.08
			570	+	−	0.16/0.08
3	$=$	\checkmark	138	−	−	
			410	+	−	3.41/18.8
			570	+	+	7.31/11.0
4	$=$	\times	138	+	+	
			410	+	+	2.41/2.07
			570	+	+	0.17/0.14

[†] indicate that the $\Lambda_c N$ 3S_1 interaction for $m_\pi = 138$ MeV is weakly attractive only at the very low energy region (about $E_{c.m.} = 3$ MeV) and then becomes repulsive as the kinetic energy increases.

[‡] The small χ^2 's compared with those of Table III imply that it is easy to reproduce the lattice QCD 3S_1 phase shifts than the coupled channel results.

³ The χ^2 shown in Table II is larger than that in Ref. [3] because of different fitting strategies. The χ^2 in Ref. [3] is obtained by fitting to the 3S_1 phase shifts, while the χ^2 in Table II includes the 3D_1 and mixing angle data as well.

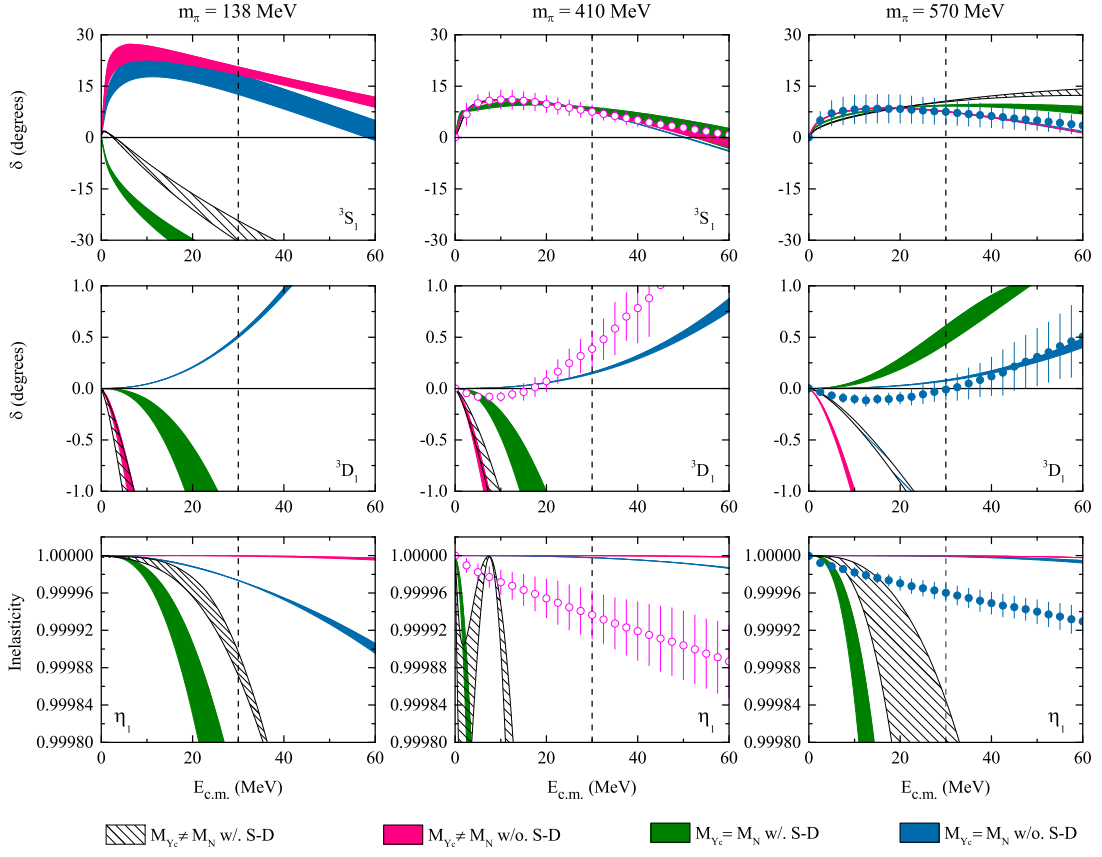


FIG. 1: $\Lambda_c N$ 3S_1 , 3D_1 phase shifts and inelasticity η_1 for different pion masses. The results are obtained by fitting to the lattice QCD $\Lambda_c N$ S -wave phase shifts for $E_{c.m.} \leq 30$ MeV. The bands are generated from the variation of Λ_F from 600 MeV to 700 MeV. Different labels denote the $\Lambda_c N$ phase shifts of strategies 1 – 4: “w/.” is the abbreviation for “with”, and “w/o.” is the abbreviation for “without”.

B. Simultaneous fits to the $\Lambda_c N$ $^3S_1 - ^3D_1$ partial waves

In this subsection, we simultaneously fit to the phase shifts of $\Lambda_c N$ 3S_1 , 3D_1 and inelasticity η_1 of the lattice QCD data for $m_\pi = 410$ and 570 MeV with a smaller energy range from threshold up to $E_{c.m.} = 5$ MeV in order to achieve a $\chi^2/\text{d.o.f.} \approx 1$. With this new strategy, we aim to check whether the covariant ChEFT approach or the non-relativistic ChEFT approach can precisely describe the lattice QCD data at low energies, where they are believed to work the best. In the covariant ChEFT, we only consider two strategies: either $M_{Y_c} \neq M_N$ or $M_{Y_c} = M_N$. The SD coupling appears naturally in the CT potentials, therefore we did not manually turn it off. The non-relativistic ChEFT approach is also applied to perform the fits for comparison. The fitted results of strategies 5 – 7, as described in Table I, are qualitatively shown in Table III and quantitatively shown in Fig. 2 and Fig. 4.

TABLE III: Phase shifts of $\Lambda_c N$ 3S_1 and 3D_1 partial waves for different pion masses based on the covariant ChEFT approach and non-relativistic ChEFT approach. The former depends on the baryon masses used, either physical or the lattice QCD M_{Y_c} and M_N or their average. These results are obtained by fitting to the phase shifts of 3S_1 , 3D_1 and inelasticity η_1 simultaneously for $E_{c.m.} \leq 5$ MeV from lattice QCD simulations, and m_π is in units of MeV. The “+” and “−” indicate the sign of $\Lambda_c N$ 3S_1 and 3D_1 partial waves phase shifts within the fitting region, where “+” and “−” stand for attractive and repulsive potentials, respectively. The values of the $\chi^2/\text{d.o.f.}$ are obtained with $\Lambda_F = 600/700$ MeV in the covariant ChEFT and $\Lambda_F = 500/600$ MeV in the non-relativistic ChEFT.

Strategy	Approach	$M_{Y_c}[\text{MeV}]/M_N$	m_π	$\delta_{^3S_1}$	$\delta_{^3D_1}$	$\chi^2/\text{d.o.f.}$
5	cov. ChEFT	\neq	138	+	−	
			410	+	−	2.65/0.92
			570	+	−	3.32/3.25
6		$=$	138	+	+	
			410	+	+	3.29/3.30
			570	+	+	5.33/5.35
7	non-rel. ChEFT		138	−	+	
			410	+	+	2.22/2.25
			570	+	+	5.37/5.45

I. Covariant ChEFT

First, we study how the use of “physical” baryon masses affects the description of the $\Lambda_c N$ interactions in the covariant ChEFT. The relevant fitting details and the corresponding values of the $\chi^2/\text{d.o.f.}$ are summarized in Table III. For strategy 5, with lattice QCD M_{Y_c}, M_N in the $\Lambda_c N$ CT potentials within the fitting region $E_{c.m.} \leq 5$ MeV, we presented the phase shifts of $\Lambda_c N$ 3S_1 and 3D_1 partial waves and inelasticity in Fig. 2. One can see that the $\Lambda_c N$ 3S_1 and 3D_1 phase shifts agree quantitatively with the lattice QCD data within uncertainties, and the asymptotic behaviors of inelasticity are in good agreement with the lattice QCD data. Comparing these results with those of strategy 6 where $M_{Y_c} = M_N$, shown in Fig. 2, one can see that the $\Lambda_c N$ 3D_1 interactions are attractive, contrary to the repulsive potential obtained in strategy 5.

In both cases, the extrapolation of the relativistic $\Lambda_c N$ 3S_1 and 3D_1 partial waves phase shifts and inelasticity to the physical point shows that the $\Lambda_c N$ interaction is attractive in the 3S_1 partial wave within the fitting region. Comparing the above results with strategy 1 (our previous study), where the $\Lambda_c N$ 3S_1 potential is repulsive, we conclude that the extrapolated phase shifts of $\Lambda_c N$ 3S_1 are not very stable.

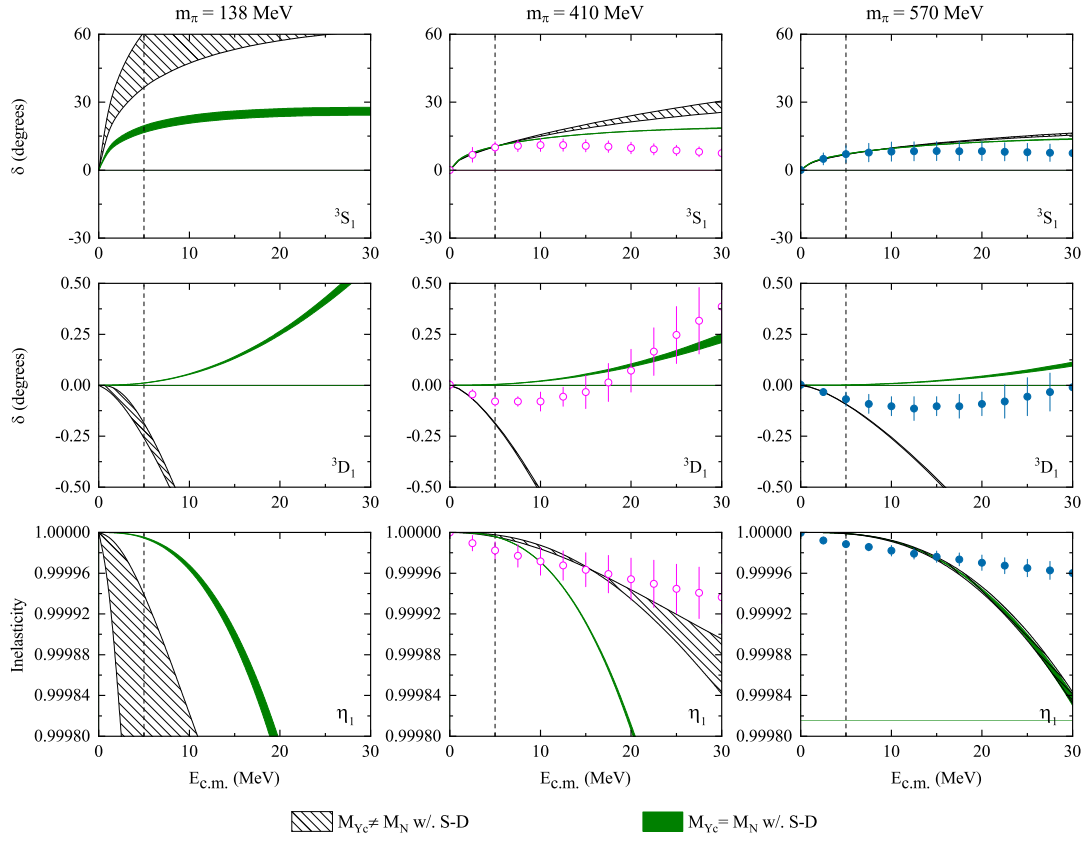


FIG. 2: Same as Fig. 1, but the results are obtained by fitting to the lattice QCD phase shifts of 3S_1 , 3D_1 partial waves and inelasticity η_1 simultaneously for $E_{c.m.} \leq 5$ MeV.

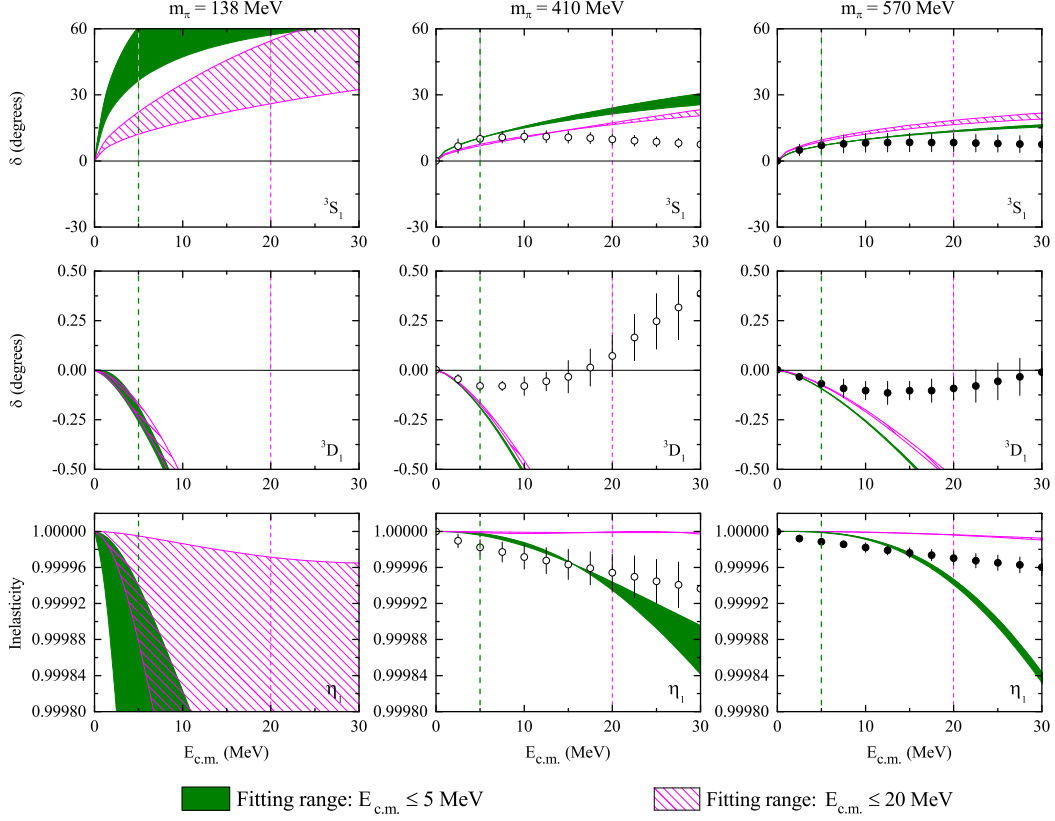


FIG. 3: $\Lambda_c N$ 3S_1 , 3D_1 phase shifts and inelasticity η_1 as functions of $E_{c.m.}$. The results are obtained by fitting to the lattice QCD δ_{3S_1} , δ_{3D_1} and η_1 simultaneously up to $E_{c.m.} \leq 5$ MeV (blue bands) and $E_{c.m.} \leq 20$ MeV (magenta bands) in covariant ChEFT.

To investigate whether the energy region fitted can affect the extrapolations, we also fitted the lattice QCD data up to $E_{c.m.} \leq 20$ MeV in the covariant ChEFT approach. The results are shown in Fig. 3 in comparison with the results obtained by fitting only up to $E_{c.m.} \leq 5$ MeV. The two fits are qualitatively consistent with each other. Only η_1 is closer to unity in the new fit. In addition, the extrapolated δ_{3S_1} and η_1 show some visible differences. At $m_\pi = 138$ MeV, δ_{3S_1} becomes smaller, and η_1 becomes more dependent on the cutoff.

2. Non-relativistic ChEFT

Focusing on the lattice QCD data with $E_{c.m.} \leq 5$ MeV, we show in Fig. 4 (the blue bands) the $\Lambda_c N$ 3S_1 , 3D_1 partial wave phase shifts and inelasticity obtained from strategy 7 in the non-relativistic ChEFT. The corresponding $\chi^2/\text{d.o.f.}$ are listed in Table III. Here, we find that the non-relativistic phase shifts of $\Lambda_c N$ 3S_1 partial wave and inelasticity are in qualitative agreement with the lattice QCD data in the region fitted. On the other hand, the $\Lambda_c N$ 3D_1 phase shifts turn out to be positive, while the lattice QCD data are negative, though quite small. This is very different from the covariant case as shown in Fig. 3, where the 3D_1 phase shifts are negative for the energy region studied. According to the previous experience in the NN sector [11, 16], the two EFTs should behave similarly in the low-energy regime, while the covariant EFT usually agrees better with the lattice QCD data than the non-relativistic EFT in the relatively high-energy regime. The present results are in conflict with such expectations to some extent. A better understanding can only be achieved once more precise lattice data with realistic uncertainties become available.

When we extrapolate the non-relativistic results to the physical point, we find that the $\Lambda_c N$ interaction is repulsive in the 3S_1 partial wave within the fitting region. Comparing these results with those of the covariant ChEFT and the left panel in Fig. 4 of Ref. [2], we again conclude that the extrapolated $\Lambda_c N$ 3S_1 interactions are not very stable, i.e., sensitive to the adopted fitting strategies.

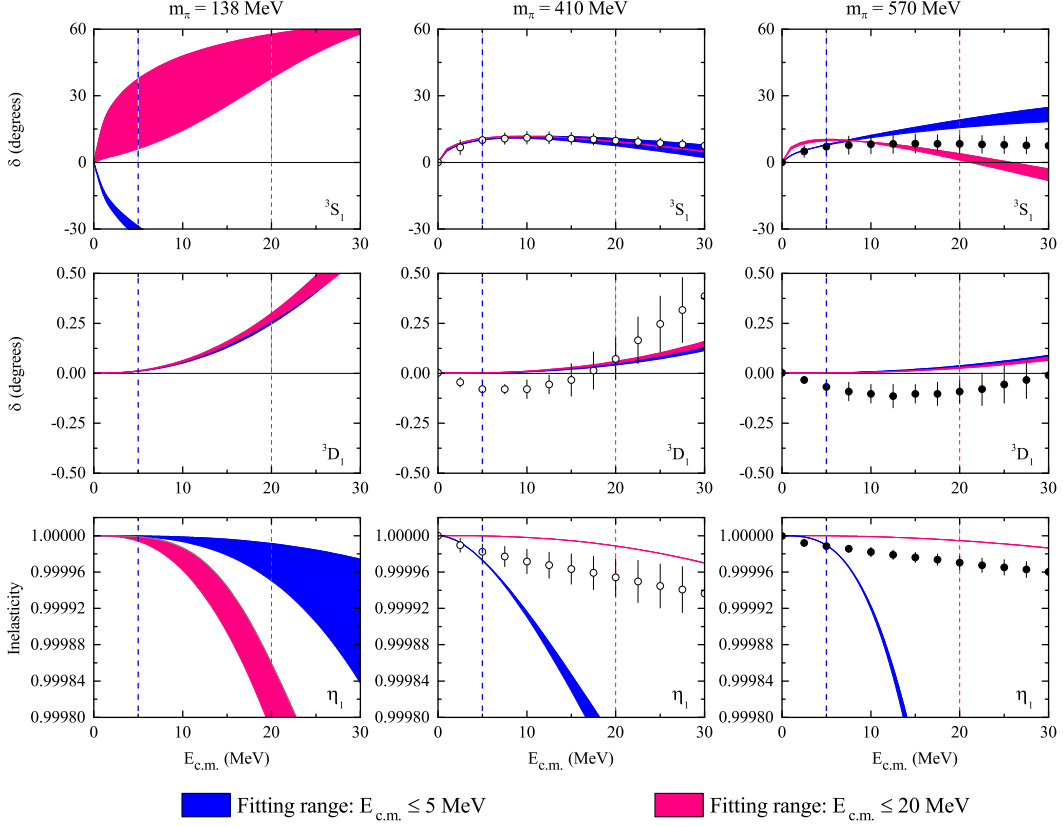


FIG. 4: Same as Fig. 3, but for the non-relativistic ChEFT.

The HB $\Lambda_c N$ 3S_1 , 3D_1 phase shifts and inelasticity with LECs obtained by fitting to the lattice QCD data up to $E_{c.m.} \leq 20$ MeV (Fit 2) are compared to those obtained by fitting only up to $E_{c.m.} \leq 5$ MeV (Fit 1) in Fig. 4. Compared to Fit 1, the descriptions of δ_{3D1} remain almost unchanged in Fit 2, but the 3S_1 phase shifts are very different. In Fit 1, δ_{3S1} increases with $E_{c.m.}$ for the case of $m_\pi = 570$ MeV, while in Fit 2, it increases with $E_{c.m.}$ for $E_{c.m.} \leq 5$ MeV and then decreases with $E_{c.m.}$, which are in better agreement with the lattice QCD simulations at least for the energy region shown in this figure. Moreover, the difference for the case of $m_\pi = 570$ MeV eventually contributes to the completely different prediction of the physical δ_{3S1} , where the phase shifts become positive in Fit 2. As for the case of $m_\pi = 410$ MeV, the two results show no qualitative difference. For the inelasticity, the results obtained in Fit 2 are closer to unity and larger than the lattice QCD simulations for the energy region fitted and become more independent on $E_{c.m.}$ as the pion mass increases.

V. CONCLUSION

The $\Lambda_c N$ $^3S_1 - ^3D_1$ interactions were studied in leading order covariant ChEFT and next-to-leading order non-relativistic ChEFT. The low-energy constants were determined in two different strategies by fitting to the HAL QCD lattice data, i.e. (a) by only fitting to the $\Lambda_c N$ 3S_1 partial wave phase shifts, (b) by a combined fit to the phase shifts of 3S_1 , 3D_1 and inelasticity η_1 . It was shown that for the first strategy, the predicted $\Lambda_c N$ 3D_1 phase shifts from the covariant ChEFT were consistent with the low-energy lattice QCD data by using lattice QCD M_{Y_c} , M_N and retaining the SD coupling in the contact potentials, while for the second strategy, one obtained results similar to those of the first strategy in the covariant ChEFT. However, the non-relativistic ChEFT predicts an attractive $\Lambda_c N$ 3D_1 interaction in both cases, which is inconsistent with the low-energy lattice QCD data. In addition, we found that the extrapolated $\Lambda_c N$ 3S_1 phase shifts in the physical region were very sensitive to the fitting strategies and the theoretical approaches used. The covariant ChEFT predicts a repulsive/attractive 3S_1 interaction depending on the fitting strategy (a)/(b), while the non-relativistic ChEFT predicts the opposite, which also depends on the energy region fitted. These results indicate that more refined lattice QCD data are needed to reach a firm conclusion about the $\Lambda_c N$ $^3S_1 - ^3D_1$ interactions.

It is necessary to point out that there are ongoing discussions on the validity of the HAL QCD method [34–36]. In our present work, we have of course assumed that the method is valid and the 3D_1 phase shifts and particularly the inelasticity are correctly extracted with the precision claimed in Ref. [18]. Hopefully, the present study can motivate a closer look at the $\Lambda_c N$ interaction

in the 3S_1 - 3D_1 coupled channel.

VI. ACKNOWLEDGEMENTS

This work was partly supported by the National Natural Science Foundation of China (NSFC) under Grants No. 11975041, No.11735003, and No.11961141004. Yang Xiao acknowledges the support from China Scholarship Council.

-
- [1] Takaya Miyamoto et al. $\Lambda_c N$ interaction from lattice QCD and its application to Λ_c hypernuclei. *Nucl. Phys.*, A971:113–129, 2018.
 - [2] J. Haidenbauer and G. Krein. Scattering of charmed baryons on nucleons. *Eur. Phys. J.*, A54(11):199, 2018.
 - [3] Jing Song, Yang Xiao, Zhi-Wei Liu, Chun-Xuan Wang, Kai-Wen Li, and Li-Sheng Geng. $\Lambda_c N$ interaction in leading-order covariant chiral effective field theory. *Phys. Rev.*, C102(6):065208, 2020.
 - [4] Xiu-Lei Ren, Kai-Wen Li, Li-Sheng Geng, Bing-Wei Long, Peter Ring, and Jie Meng. Leading order relativistic chiral nucleon-nucleon interaction. *Chin. Phys.*, C42(1):014103, 2018.
 - [5] Kai-Wen Li, Xiu-Lei Ren, Li-Sheng Geng, and Bing-Wei Long. Leading order relativistic hyperon-nucleon interactions in chiral effective field theory. *Chin. Phys.*, C42(1):014105, 2018.
 - [6] Xiu-Lei Ren, Chun-Xuan Wang, Kai-Wen Li, Li-Sheng Geng, and Jie Meng. Relativistic Chiral Description of the 1S_0 Nucleon–Nucleon Scattering. *Chin. Phys. Lett.*, 38(6):062101, 2021.
 - [7] Jing Song, Kai-Wen Li, and Li-Sheng Geng. Strangeness $S = -1$ hyperon-nucleon interactions: Chiral effective field theory versus lattice QCD. *Phys. Rev.*, C97(6):065201, 2018.
 - [8] Xiu-Lei Ren, Kai-Wen Li, and Li-Sheng Geng. Towards a relativistic formulation of baryon-baryon interactions in chiral perturbation theory. *Nucl. Phys. Rev.*, 34:392, 2017.
 - [9] Kai-Wen Li, Tetsuo Hyodo, and Li-Sheng Geng. Strangeness $S = -2$ baryon-baryon interactions in relativistic chiral effective field theory. *Phys. Rev.*, C98(6):065203, 2018.
 - [10] Chun-Xuan Wang, Li-Sheng Geng, and Bingwei Long. Renormalizability of leading order covariant chiral nucleon-nucleon interaction. *Chin. Phys. C*, 45(5):054101, 2021.
 - [11] Qian-Qian Bai, Chun-Xuan Wang, Yang Xiao, and Li-Sheng Geng. Pion-mass dependence of the nucleon-nucleon interaction. *Phys. Lett.*, B809:135745, 2020.
 - [12] Zhi-Wei Liu, Jing Song, Kai-Wen Li, and Li-Sheng Geng. Strangeness $S = -3$ and $S = -4$ baryon-baryon interactions in relativistic chiral effective field theory. *Phys. Rev.*, C103(2):025201, 2021.
 - [13] Jing Song, Zhi-Wei Liu, Kai-Wen Li, and Li-Sheng Geng. Test of the hyperon-nucleon interaction within leading order covariant chiral effective field theory. *Phys. Rev. C*, 105(3):035203, 2022.
 - [14] Zhi-Wei Liu, Kai-Wen Li, and Li-Sheng Geng. Strangeness $S = -2$ baryon-baryon interactions and femtoscopic correlation functions. *arXiv: 2201.04997*, 2022.
 - [15] Jun-Xu Lu, Chun-Xuan Wang, Yang Xiao, Li-Sheng Geng, Jie Meng, and Peter Ring. Accurate Relativistic Chiral Nucleon-Nucleon Interaction up to Next-to-Next-to-Leading Order. *Phys. Rev. Lett.*, 128(14):142002, 2022.
 - [16] Qian-Qian Bai, Chun-Xuan Wang, Yang Xiao, Jun-Xu Lu, and Li-Sheng Geng. Nucleon-nucleon interaction in the $3S_1$ - $3D_1$ coupled channel for a pion mass of 469 MeV. *Phys. Lett. B*, 833:137347, 2022.
 - [17] J. Haidenbauer and G. Krein. Comment on “ $\Lambda_c N$ interaction in leading order covariant chiral effective field theory”. *arXiv: 2101.07160*, 2021.
 - [18] Takaya Miyamoto. *Charmed baryon interaction from lattice QCD and its application to charmed hypernuclei*. PhD thesis, Kyoto U., 2019.
 - [19] J. Haidenbauer, G. Krein, and T. C. Peixoto. Femtoscopic correlations and the $\Lambda_c N$ interaction. *Eur. Phys. J.*, A56(7):184, 2020.
 - [20] Henk Polinder, Johann Haidenbauer, and Ulf-G. Meissner. Hyperon-nucleon interactions: A Chiral effective field theory approach. *Nucl. Phys.*, A779:244–266, 2006.
 - [21] H. P. Stapp, T. J. Ypsilantis, and N. Metropolis. Phase shift analysis of 310-MeV proton proton scattering experiments. *Phys. Rev.*, 105:302–310, 1957.
 - [22] H. Polinder, J. Haidenbauer, and U. G. Meissner. Strangeness $S = -2$ baryon-baryon interactions using chiral effective field theory. *Phys. Lett.*, B653:29–37, 2007.
 - [23] J. Haidenbauer and Ulf-G. Meissner. The Jülich hyperon-nucleon model revisited. *Phys. Rev.*, C72:044005, 2005.
 - [24] J. Haidenbauer, Ulf-G. Meissner, A. Nogga, and H. Polinder. The Hyperon-nucleon interaction: Conventional versus effective field theory approach. *Lect. Notes Phys.*, 724:113–140, 2007.
 - [25] J. Haidenbauer and U. G. Meissner. Predictions for the strangeness $S = -3$ and -4 baryon-baryon interactions in chiral effective field theory. *Phys. Lett.*, B684:275–280, 2010.
 - [26] J. Haidenbauer. Baryon-baryon interactions from chiral effective field theory. *Nucl. Phys.*, A914:220–230, 2013.
 - [27] J. Haidenbauer, S. Petschauer, N. Kaiser, U. G. Meissner, A. Nogga, and W. Weise. Hyperon-nucleon interaction at next-to-leading order in chiral effective field theory. *Nucl. Phys.*, A915:24–58, 2013.
 - [28] J. Haidenbauer, Ulf-G. Meissner, and S. Petschauer. Strangeness $S = -2$ baryon–baryon interaction at next-to-leading order in chiral effective field theory. *Nucl. Phys.*, A954:273–293, 2016.

- [29] J. Haidenbauer, S. Petschauer, N. Kaiser, Ulf-G Meissner, and W. Weise. Scattering of decuplet baryons in chiral effective field theory. *Eur. Phys. J.*, C77(11):760, 2017.
- [30] J. Haidenbauer, U. G. Meissner, and A. Nogga. Hyperon–nucleon interaction within chiral effective field theory revisited. *Eur. Phys. J.*, A56(3):91, 2020.
- [31] Johann Haidenbauer, Andreas Nogga, and Isaac Vidaña. Predictions for charmed nuclei based on $Y_c N$ forces inferred from lattice QCD simulations. *Eur. Phys. J.*, A56(7):195, 2020.
- [32] V. G. Kadyshevsky. Quasipotential type equation for the relativistic scattering amplitude. *Nucl. Phys.*, B6:125–148, 1968.
- [33] Takaya Miyamoto. Coupled-channel $\Lambda_c N - \Sigma_c N$ interaction from lattice QCD. *PoS, Hadron2017*:146, 2018.
- [34] Takumi Iritani, Sinya Aoki, Takumi Doi, Testuo Hatsuda, Yoichi Ikeda, Takashi Inoue, Noriyoshi Ishii, Hidekatsu Nemura, and Kenji Sasaki. Are two nucleons bound in lattice QCD for heavy quark masses? Consistency check with Lüscher’s finite volume formula. *Phys. Rev. D*, 96(3):034521, 2017.
- [35] Silas R. Beane et al. Comment on ”Are two nucleons bound in lattice QCD for heavy quark masses? - Sanity check with Lüscher’s finite volume formula -”. *arXiv: 1705.09239*, 2017.
- [36] Takumi Iritani, Sinya Aoki, Takumi Doi, Tetsuo Hatsuda, Yoichi Ikeda, Takashi Inoue, Noriyoshi Ishii, Hidekatsu Nemura, and Kenji Sasaki. Consistency between Lüscher’s finite volume method and HAL QCD method for two-baryon systems in lattice QCD. *JHEP*, 03:007, 2019.